

# One Dimensional Plasmonic Grating: High Sensitive Biosensor

Tahir Iqbal<sup>1</sup> · Sumera Afsheen<sup>2</sup>

Received: 2 January 2016 / Accepted: 27 March 2016 / Published online: 7 April 2016  
© Springer Science+Business Media New York 2016

**Abstract** We report a simple 1D grating device fabrication on ~50 nm gold (Au) film deposited on glass, which is employed as a high performance refractive index (RI) sensor by exploiting the surface plasmon polaritons (SPP) excited by the grating device along the Au/analyte interface. A finite element analysis (FEA) method is employed to maximize the sensitivity of the sensor for a fixed period and thickness of a gold film and its close correspondence with experiment has given the insight for high sensitivity and enhanced transmission. Significantly, in the context of economic design and performance, it is shown that an optimally designed and fabricated 1D grating can be as sensitive as 524 nm/RIU (linearity RI= 1.33303 to 1.47399), which is remarkably higher than existing reports operating in a similar wavelength region.

**Keywords** 1D grating · Surface plasmon polaritons · Refractive index · Gold film · Finite element analysis (FEA)

## Introduction

Optical means of sensing is a reliable technique which has proven its potential in recent years, especially in the context of plasmonic sensors for a plethora of applications depicting

high throughput and label-free detections, having been developed with commercially existing products [1, 2].

The SPPs are sensitive to the small variations in the refractive index (RI) at the surface of the metal that supports them which is the basis for most of the biosensing applications [3, 4]. Plasmonic sensors based on periodic metal nanostructures [5, 6] (1D/2D gratings and their derivatives) have attracted a lot of attention due to their simplicity and scalability with two main resonance modes, namely a SPP mode known as the Bloch mode and a guided/slit mode known as the Fabry-Perot (FP) mode. The SPP mode depends on the incidence angle of TM wave, period and the order of the resonance [5, 6], while the FP mode depends on the geometrical parameters of the single slit system [7]. The detection sensitivity depends on the surface area and accessibility, which are less for the FP mode than the SPP modes. The coupling efficiency of a grating device [8] also strongly influences the sensitivity of a plasmonic based biosensor.

Furthermore, for cost effective and scalable fabrication purposes, it is appropriate to improve the sensitivity of a 1D grating by employing the SPP mode in the detection, which is of course less investigated in the context of RI sensor. In this context, the sensitivity of the grating device is maximized by tuning the grating parameters (at a fixed period) through numerical simulation and it is shown that such optimum performance can be achieved practically.

The sensitivity (shift in wavelength over refractive index per unit (RIU)) of the 1D grating devices presented in this work is higher than earlier reported for plasmonic biosensors containing complex architecture [9–11]. For example, nanorods/tubes (225 nm/RIU [9]), elongated Au discs (200 nm/RIU [10]), and Au nanoparticles (450 nm/RIU [11]) employ localized surface plasmon resonance (LSPR), while nanohole arrays (333 nm/RIU [12]) use extraordinary optical transmission (EOT) to detect the RI. When it comes to a 1D grating, the FP mode is employed to detect the RI

---

✉ Tahir Iqbal  
tahir.awan@uog.edu.pk; tiqbal02@qub.ac.uk

<sup>1</sup> Department of Physics, Faculty of Science, University of Gujrat, Hafiz Hayat Campus, Gujrat 50700, Pakistan

<sup>2</sup> Department of Zoology, Faculty of Science, University of Gujrat, Hafiz Hayat Campus, Gujrat 50700, Pakistan

and a sensitivity of 525 nm/RIU [7] is obtained using simulations. Homola and Piliarik [3] had suggested a theoretical sensitivity of 250–400 nm/RIU for a grating coupled sensor (see appendix Table 2 for a comparison of different studies within the context of plasmonic based bio-sensing). So, it can be concluded that LSPR are useful when nanoparticles are used as sensor. The Bloch mode is utilized when periodic nanostructures are fabricated on gold metallic film of thickness around 50 nm, whereas FP mode becomes more effective, when the film thickness is large i.e. greater than 200 nm. Hence, in the present case Bloch mode have more impact on the sensitivity.

Many other plasmonic nanostructures have been reported [13–21] to detect change in RI. Note that employing the SPP mode of a 1D grating for detection can be as much as nearly 1.3 times more sensitive on average than the other studies referenced while also using a thinner Au film of ~50 nm.

Furthermore, in the context of RI detection most biodetectors have to operate in an aqueous environment, which inhibits the resonance wavelength  $\lambda_{res}$  shifting into IR region. By increasing the periodicity to 630 nm in the grating device, an even higher sensitivity (637 nm/RIU) can be achieved, while the SPP resonance wavelength  $\lambda_{res}$  shifts into the IR spectral region ( $\lambda_{res} = 825\text{--}850$  nm, results not shown).

A simple design of 1D plasmonic grating is presented here which measures the RI change in the environment. The results are well corroborated with finite element analysis (FEA) and explained by field distributions associated with the surface plasmon resonance (SPR) in accordance with the grating geometry.

## Methods

### Sample Preparation

A cover glass slip (22 × 22 mm) was washed in deionized water and used as substrate. After drying, the sample was inserted into a vacuum chamber to deposit the Au film via a thermal evaporator. A 50-nm gold thin film is deposited on the glass substrate using a thermal evaporator in a high vacuum of  $\sim 10^{-6}$  Torr to avoid any oxidation and collision between the vapor and surroundings. The Au film thickness is monitored with a quartz crystal which is mounted inside the chamber.

### Device Fabrication and Analyte Composition

A one-dimensional (1D) grating device with periodicity  $\Lambda = 525$  nm, and with sub-wavelength slit width  $a = 272$  nm, is patterned on the Au thin film using FIB etching using FEI Nov. 600i dual-beam operating at 48 pA beam current of aperture 19 nm. The fabricated device

is characterized via a scanning electron microscope (SEM, JEOL 6500 FESEM).

This device was then encapsulated by another thin glass slide such that a space is created for the analyte to be inserted for the measurement of the relevant refractive index change using the far-field optical setup.

In order to obtain an analyte of controlled refractive index, a mixture of glycerine and deionised (DI) water was employed in various ratios to produce  $n = 1.33303, 1.33880, 1.34481, 1.37070, 1.38413, 1.42044, 1.45085$  and  $1.47399$  as shown in Table 1. Great care was made to get a homogeneous solution.

## Experimental Setup

The transmission spectra from the plasmonic device were tested using a white-light source (70 W, QTH halogen lamp) via the newly designed and built far-field optical characterization setup. The complete detail is described in ref [23].

## Physical Background and Theory

Figure 1 shows the schematic of a 1D grating device on glass substrate, where  $t$  is the thickness of Au,  $a$  is the slit width and  $\Lambda$  is the periodicity. This 1D-Au grating device on glass substrate was used to detect small change in RI (analyte). The optical properties of gold are adopted from reference [24]. A TM plane wave ( $E_x$  and  $E_y$  were in plane while  $H_z$  was orthogonal to the simulation plane) illuminates at normal incidence (Fig. 1). In the modelling, the computational domain is bounded by perfectly matched layers (PMLs) on the top and bottom of the unit cell and by periodic boundary conditions along the grating periodicity with a mesh size of 20 nm. The plasmonic grating is covered by an over-layer of analyte, having thickness  $h$  and refractive index  $n_h$ .

**Table 1** Refractive index of glycerine-water solution at room (see ref [22])

No.	Refractive index ( $n$ )	Glycerine % by weight
1.	1.33303	0
2.	1.33880	5
3.	1.34481	10
4.	1.37070	30
5.	1.38413	40
6.	1.42044	65
7.	1.45085	85
8.	1.47399	100

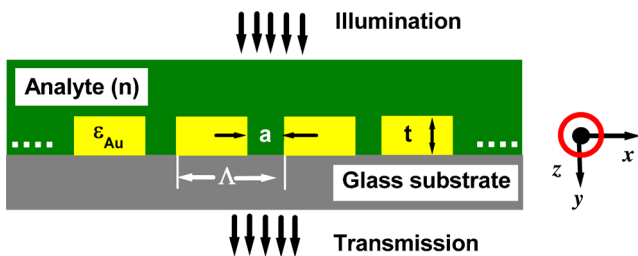


**Fig. 1** Schematic of the 1D grating under normal incidence.  $\epsilon_{Au}$ ,  $n$  are the permittivity and RI of the gold and analyte, respectively.  $\Delta$ —periodicity,  $a$ —slit width,  $t$ —thickness of Au film

In a 1D grating the SPP mode occurs at  $\lambda_{res}$  (resonance wavelength) when the phase-matching condition is satisfied between the incident TM light and the periodicity of the grating. For a planar metal/dielectric interface, the  $\lambda_{res}$  for TM polarized light at normal incidence can be described as [5]

$$\lambda_{res} = \Delta \sqrt{\frac{\epsilon_m \epsilon_d}{\epsilon_m + \epsilon_d}} \quad (1)$$

where  $\epsilon_m$  and  $\epsilon_d$  are the permittivity of the metal and the adjacent dielectric, respectively.

Note that in this work only zero-order transmission through the grating device was obtained to evaluate the SPP mode resonance corresponding to the Au/analyte interface, hence eliminating the need for prism coupling, which is less practical with reference to operation issues.

The aim of this study is to employ the SPP mode (at Au/analyte interface) to detect the RI at its maximum sensitivity which is given by

$$S_\lambda = \frac{\Delta \lambda_{res}}{\Delta n} \quad (2)$$

where  $\Delta \lambda_{res}$  and  $\Delta n$  are changes in resonance wavelength and RI, respectively. Therefore, the grating parameters (slit width) are tuned for a fixed periodicity ( $\Delta = 525$  nm) in the device to optimize sensitivity for the SPP mode along the Au/analyte interface.

In order to see behaviour of the SPP mode, which is dependent on dielectric constant of the Au/dielectric (analyte) interface, it is important to understand that such grating devices have two interfaces (i) Au/substrate (here in the present case it is glass) and (ii) Au/superstrate (analyte). Hence, depending upon the RI of both interfaces, namely Au/analyte ( $I_1$ ) and Au/glass ( $I_2$ ) both support a propagating SPP (Bloch) mode. The coupling of incident light into the SPP occurs at  $I_1$  and  $I_2$  for zero order plasmonic mode which can be seen from the dispersion plot (Fig. 2), yielding  $\sim 1.69$  and  $\sim 1.55$  eV for  $n = 1.33303$ ,  $1.47399$  at  $I_1$  and  $\sim 1.51$  eV at  $I_2$ . Notably, the spectral location of these states derived from Fig. 2 falls within  $\sim 10\%$  error for  $2\pi/\Delta$  periodicity [6].

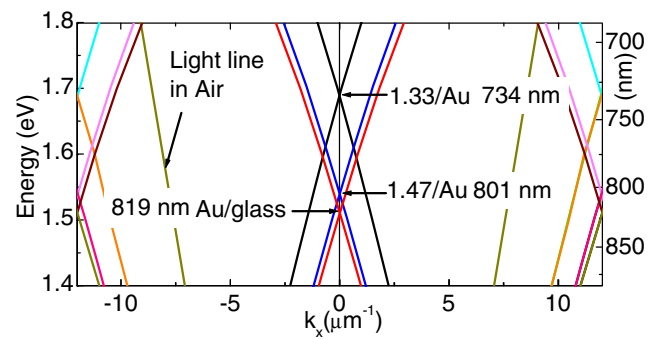


**Fig. 2** A theoretical dispersion plot for a 1D grating for period 525 nm, where zero-order resonance conditions for Au/analyte and Au/glass interfaces are annotated alongside light line,  $\omega = ck/(\epsilon_d)^{1/2}$ . Refractive index of glass is taken as 1.5

### Results and Discussion

Here, zeroth order transmission spectra  $T(\lambda, n)$  are presented in Fig. 3a, whereas simulated results are presented in Fig. 3b. The SEM of the grating structure is shown in inset of Fig. 3a and the field profiles to make other plasmon related insights, viz resonance at  $I_1$  is shown in inset of Fig. 3b. It is noteworthy that the grating parameters are optimized in such a way that

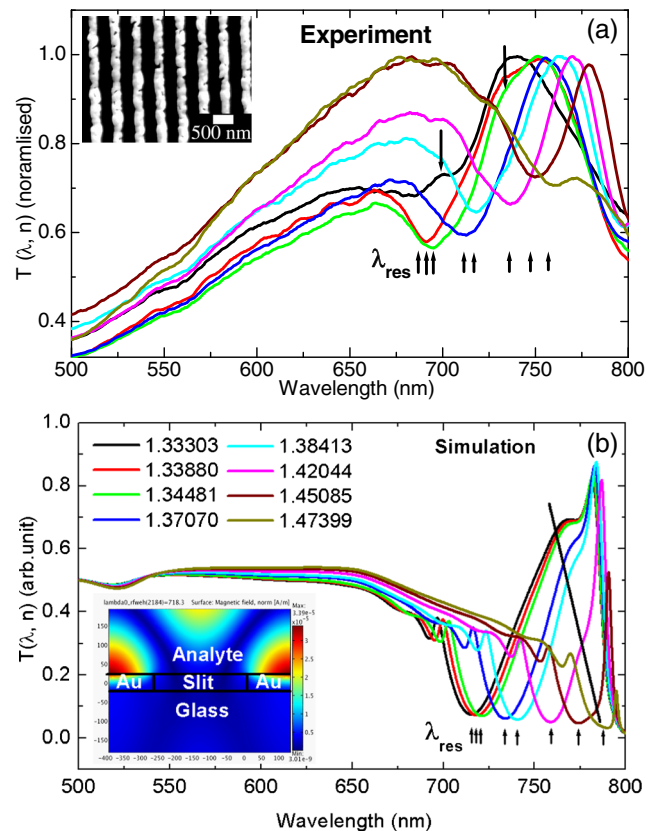


**Fig. 3** Zero-order transmission spectra from a 1D grating for various analyte RI (a) experiment (b) simulation. Inset in (a) SEM image of 1D grating and (b) simulated  $|\vec{H}|$  A/m distribution at  $\lambda_{res} = 718.3$  nm for a RI 1.33880, respectively

SPP mode is achieved at  $I_1$ . The SPP mode,  $\lambda_{res}$  for  $I_1$  is identified (arrows on Fig. 3) for each ‘RI’ via inspecting the magnetic field ( $|\vec{H}|$ ) distributions against wavelength and the representative  $|\vec{H}|$  (inset Fig. 3b) for one unit cell. Note that  $|\vec{H}|$  represents the strength of the local surface current flowing in between the accumulations of surface-charge; such a field profile has been previously reported by Grande et al. [7]. The field profile indicates that the penetration depth is greater for the analyte than Au, consistent with characteristics well known in the literature [5].

In line with the simulation, a series of experimental zeroth order transmission,  $T(\lambda, n)$  spectra were obtained which are shown in Fig. 3a, where the features on the spectra are reproducible from different samples of similar grating parameters. The SEM image of a grating (inset of Fig. 3a), yielding  $\Lambda = 525 \pm 10$  nm, and  $a = 272 \pm 15$  nm. As the RI of environment increases, due to the change in the effective RI the resonance wavelength between the light wave and the SPPs also increases, reflected in a red-shift of  $\lambda_{res}$  in  $T(\lambda, n)$  spectra shown in Fig. 3a, b [25]. There is promising agreement between experimental results (Fig. 3a) and simulated results (Fig. 3b) corresponding to each RI.

It is worth mentioning that the individual grains of Au film (diameter  $\sim 60 \pm 15$  nm) can possess LSPR, depending on their size [26]. Nominal 35–100 nm diameter Au nanoparticles have a LSPR peak wavelength ranging from  $\sim 535$ –595 nm [27], and hence an infringement from the LSPR can be ignored [26] as the operational wavelength for the device is above 650 nm in wavelength.

The spectra in Fig. 3b are simulated for a ‘perfect grating’ under a TM plane wave at normal incidence, while the experiment (Fig. 3a) is performed on a morphologically rough grating with an illumination cone angle of  $\sim 32^\circ$  (NA of the focusing objective). These discrepancies may cause disparity between the experiment and the simulation when it comes to the spectral location and the shape of resonances [9, 28]. The detection accuracy primarily depends on the type of the detector (spectrometer) used. Furthermore, it depends that the blazed wavelength range for the grating used in the spectrometer where the detector have more detection efficiency. In the present case, the spectrometer used has the highest detection accuracy (efficiency) i.e. in infrared (IR) and near infrared (NIR) where the SPPs are excited and hence detected by the detector more efficiently.

Here, co-plotted zero-order transmission spectra from simulation and experimental results  $T(\lambda, 1.33880)$  are shown in Fig. 4 depicting an explicit re-traceability where the corresponding spectral features are numbered (1, 2 and 3). The dip in the  $T(\lambda, n)$  due to the SPP (Bloch) mode at  $I_1$  (see inset Fig. 4a) is explained on the basis of diffraction [29] or interference [28] or FDTD [30], while a disagreement in terms of general wavelength shift is also seen [31].

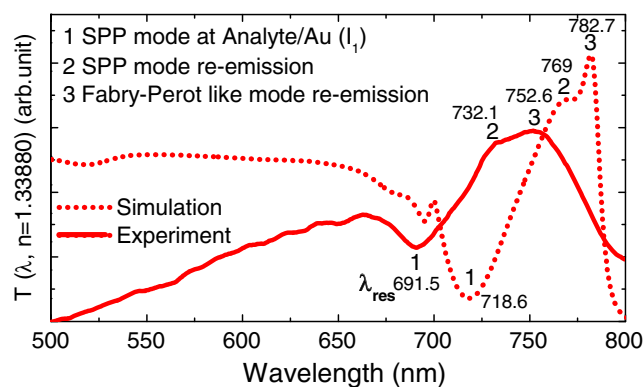


**Fig. 4** Zero-order transmission spectra of simulation and experiment are co-plotted for RI = 1.33880

Xie et al. [30] note that the periodicity governs the interaction between adjacent slits in terms of creation and subsequent radiation of strong dipoles into the slit aperture at the edges of the slits. Note that EOT is interpreted to originate from diffraction and FP modes [32], or surface modes (at both the interfaces) and FP modes [30]. In the present context feature 2 corresponds to the emission of 1 (at  $I_1$ ) which can be treated as EOT for a grating with a mark-to-space ratio of unity. Re-emitted peaks for  $n = 1.33303$  are clear (see down-arrows on Fig. 3a) while for  $n = 1.34481$  a signature is identified (Fig. 4). A FP-like mode in the slit at  $\sim 740$  nm for  $n = 1.33880$  has given rise to feature 3. A slight red-shift of 3 with increasing RI explains that this mode is not very useful for biodetection, which requires much stronger coupling [7]. A further increase in the RI red-shifts the features 1 and 2 (see dotted line in Fig. 3b) [25]. However, as peak 2 red-shifts the composite peak (2 and 3) intensity declines, which is an important observation. Notably, this is consistent in simulation and experiment. The computed field profiles of the  $n = 1.33303$  and  $n = 1.47399$  clarify the role played by the SPP mode at  $I_1$  and  $I_2$  in decreasing the intensity of the composite peak. The boundary conditions at the top and bottom of the slit favour the launching of a strong guided mode into the slit waveguide.

As earlier indicated [30], the SPP modes excited at the top and bottom facets of the metal film, as well as resonant FP modes, play major roles in determining the transmission. Another study suggests that the surface mode can enhance or inhibit light transmission [33]. As the analyte RI approaches that of glass, the excitation of the SPP mode at  $I_2$  begins to be favoured, while  $I_1$  still exists. Interestingly, this feature did not alter the sensitivity. Although not shown here for the sake of conciseness, when the RIs of dielectric at  $I_1$  and  $I_2$  are equal i.e. RI = 1.5, the composite peak almost disappears. Under illumination, the light couples into surface waves at both the interfaces which subsequently weakens the transmission substantially [30]. With reference to Xie et al.’s work [30], the coupling between two SPP modes on either side of the metal is a strong function of film thickness which is



explicitly evidenced here; competition between  $I_1$  and  $I_2$  is observed. The competition between the two modes can be also be seen in the dispersion curve (Fig. 2) when the RI of analyte approaches that of glass and there is a possibility of exciting wide-band SPP modes at  $I_1$  and  $I_2$ .

Moving on to the focus of present case, a high angle of incidence creates strong coupling between the incident plane wave and the SPs i.e. with the wave vector nearly parallel to the surface. Pang et al. [34] report that a normal incidence produces a strong interaction between various SPP modes in a 2D-hole array, while noting the higher sensitivity in angular modulation.

Since the sensitivity is inversely proportional to the integer numbers of the corresponding SPP modes, the lowest order modes are most sensitive to the change in the RI of the dielectric [35]. By considering these  $\lambda_{res}$  under normal incidence for zero-order transmission, which are extracted from experiment, simulation and theory (Eq. 1) and plotted against RI in Fig. 5. The sensitivities are annotated on the image. Significantly, within  $n \sim 1.33$ – $1.47$  this sensor has shown linearity notably similar to the prism-based sensor [25] despite the non-linear relation (Eq. 1). The plausible reasons for the slight disagreement between simulation and experiment have been addressed earlier. An earlier report (McPhillips et al. [9]) has a discrepancy of  $\sim 125$  nm (value estimated from the graph) between experiment and simulation, while here it is  $\sim 30$  nm for similar RI ( $\sim 1.333$ ). However, the deviation ( $\sim 8.5\%$  for  $n \sim 1.33$ ) of theory and simulation is not unreasonable.

In addition to comparison with previous theoretical studies of sensitivity ( $\sim 250$ – $400$  nm/RIU [3]) those based on LSPR sensors [21], antisymmetric [20], quadrupole [36], multimode (quadrupole or mixed) [19], and waveguide coupled grating resonance sensors [14] have shown sensitivities in the range of  $\sim 90$ – $350$  nm/RIU (also see appendix Table 2).

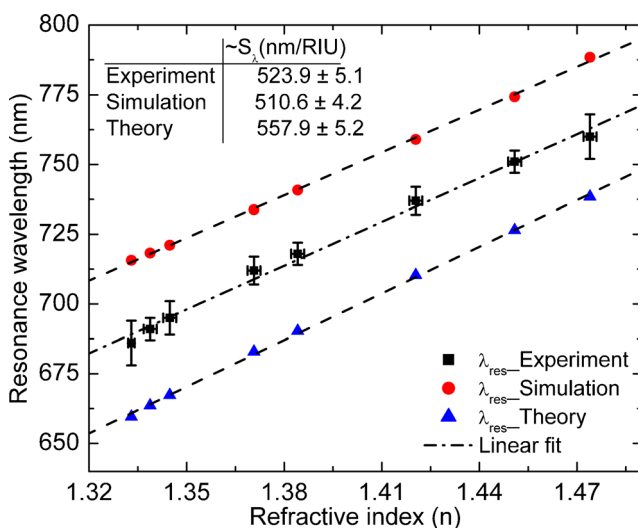


**Fig. 5** The SPP resonance wavelengths  $\lambda_{res}$  against RI from experiment, simulation and theory

On the other hand, the sensor based on FP modes has a simulated sensitivity (525 nm/RIU [7]) similar to that of present study with a film thickness of 220 nm. In contrast, the present case employs less than one fourth of the film thickness which is vital for cost effective devices. This comparative analysis conveys an important message, that the SPP mode, if appropriately employed from an optimized 1D grating to detect RI is highly competitive with other SPP-based sensors that either have more complex geometry or utilize a greater quantity of expensive material.

### Conclusions

It is shown that the geometrically sensitive SPP mode of a grating can be employed for efficient detection of RI, where an analytically optimized grating is fabricated and its sensitivity against RI is tested for a range of biomatter-media. The observed EOT is explained on the basis of a leaky wave, and FP-like modes within the slits. As indicated by a computational study [30] with notable disagreements [31, 32] about the role of SPs in EOT, based on the present results from the simulation and experiment the excitation of SPs at two interfaces on the either side of the slits in fact reduces the transmission significantly.

The experimental results are compared with FEA simulation and theoretical values which are in agreement with each other with a deviation in sensitivity of  $\sim 4\%$ . The resonance behaviour in response to the RI change of the surroundings is replicated and explained thoroughly by the modelling. The sensitivity is  $\sim 1.3$  times higher than earlier reports operating under various resonance states. Importantly, the present results are reproducible from different sample gratings for all the analytes.

Furthermore, the grating is subjected to washing with DI water after every test of RI and it is able to obtain the spectrum that corresponds to a clean grating confirming its reusability except for case of the liquids that are permanently adsorbed onto the gold surface. For an optimum choice of grating parameters, 1D gratings can be effectively employed to attain very high sensitivity and are well suited for miniaturization when employed under normal incidence. The last and most important observation is that the SPP-based biosensor is independent of the height (depth) of the analyte (results not shown here) to be detected in contrast to the FP based biosensor. Such grating devices have many other applications as well [37, 38].

**Acknowledgments** Dr Tahir Iqbal greatly acknowledge to all concern quarters for their technical and financial help to complete this research work.

## Appendix

**Table 2** Sensitivity of various detectors with details those appeared in the literature

Type of device	Mode	$\sim S_\lambda$ (nm/RIU)	Parameter (nm)	$\lambda_{\text{res}}$ (nm) (refractive index)	Ref
1D grating	Surface/Bloch mode	524 <sup>b</sup> ; 511 <sup>a</sup>	Film thickness = 50	680 (1.33303)	This study
Nanorods/ tubes	Localized surface plasmons (LSPs)	225	Length = 120	759 <sup>c</sup> (1.333)	J.McPhillips et al.
Au nanoparticles,	LSPs	450 <sup>a, c</sup>	Aspect ratio = 3, Diameter = 20	$\sim 780^c$ (1.33)	M.M. Miller et al.
Elongated discs	LSPs	200 <sup>b</sup>	Aspect ratio = 7, Diameter = 137, thickness = 20		P. Hanarp et al.
Nanohole arrays	Extraordinary optical transmission (EOT)	333 <sup>b</sup>	Diameter = 150, period = 450	678 (1.332)	A. De Leebeek et al.
1D grating	Fabry-Perot	$\sim 525^a$	Au thickness = 220 <sup>a</sup>	730 <sup>c</sup> (1.33)	M. Grande et al.
1D grating array, biofunctional material	EOT	668 <sup>b</sup>	150, period = 600	807 (1.32)	K.L. Lee et al.
1D-Au and 1D-SiN <sub>x</sub> double grating	Guided mode resonance slotted section	$\sim 720^a$	Au thickness = 200 SiN <sub>x</sub> thickness = 500	752.6 (1.00) period = 750 nm (1.00)	M. Hong et al.
Grating	Surface/Bloch mode	250-400 <sup>d, c</sup>	NA	680 <sup>d, c</sup>	J. Hamola et al.

<sup>a</sup> Simulation

<sup>b</sup> Experiment

<sup>c</sup> Approximated from the graph

<sup>d</sup> Theoretical

J. McPhillips, A. Murphy, M. P. Jonsson, W. R. Hendren, R. Atkinson, F. Hook, A. V. Zayats, and R. J. Pollard, *Acs Nano* **4**, 2210 (2010)

M. M. Miller and A. A. Lazarides, *J. Phys. Chem. B* **109**, 21556 (2005)

P. Hanarp, M. Kall, and D. S. Sutherland, *J. Phys. Chem. B* **107**, 5768 (2003)

A. D. Leebeek, L. K. S. Kumar, V. d. Lange, D. Sinton, R. Gordon, and A. G. Brolo, *Anal. Chem.* **79**, 4094 (2007)

H. J. Lezec, A. Degiron, E. Devaux, R. A. Linke, L. Martin-Moreno, F. J. Garcia-Vidal, and T. W. Ebbesen, *Science* **297**, 820 (2002)

A. J. Haes, S. Zou, G. C. Schatz, and R. P. V. Duyne, *J. Phys. Chem. B* **108**, 109 (2004)

L. Pang, G. M. Hwang, B. Slutsky, and Y. Fainman, *Appl. Phys. Lett.* **91**, 123112 (2007)

M. Grande, R. Marani, F. Portincasa, G. Morea, V. Petruzzelli, A. D'Orazio, V. Marrocco, D. de Ceglia, and M. A. Vincenti, *Sensor. Actuat. B-Chem.* **160**, 1056 (2011)

K.-L. Lee, C.-W. Lee, W.-S. Wang, and P.-K. Wei, *J. Biomed. Opt.* **12**, 044023 (2007)

M. Hong, L. Shi, H. Li, Y. Du, Z. Wang, Y. Weng, and D. Li, *Opt. Commun.* **285**, 5480 (2012)

J. Homola and M. Piliarik, *Surface plasmon resonance (SPR) sensors*, Vol. 4 (2006)

## References

- Anker JN et al (2008) Biosensing with plasmonic nanosensors. *Nat Mater* **7**:442–453
- Cooper MA (2002) Optical biosensors in drug discovery. *Nat Rev Drug Discov* **1**:515–528
- Homola J, Piliarik M (2006) Surface plasmon resonance based sensors springer series on chemical sensors and biosensors., pp 45–67
- Vempati S, Iqbal T, Afsheen S (2015) Non-universal behavior of leaky surface waves in a 1D asymmetric plasmonic grating. *J Appl Phys* **118**:043103
- Raether, H (1988) Surface plasmons on smooth and rough surfaces and on gratings. Springer-Verlag, Berlin Heidelberg
- Ebbesen TW, Lezec HJ, Ghaemi HF, Thio T, Wolff PA (1998) Extraordinary optical transmission through sub-wavelength hole arrays. *Nature* **391**:667–669
- Grande M et al (2011) Asymmetric plasmonic grating for optical sensing of thin layers of organic materials. *Sensor Actuat B-Chem* **160**:1056–1062
- Iqbal T, Afsheen S (2015) Extraordinary optical transmission: Role of the slit width in 1D metallic grating on higher refractive index substrate. *Curr Appl Phys* **16**(1):453–458
- McPhillips J et al (2010) High-performance biosensing using arrays of plasmonic nanotubes. *ACS Nano* **4**:2210–2216
- Hanarp P, Kall M, Sutherland DS (2003) Optical properties of short range ordered arrays of nanometer gold disks prepared by colloidal lithography. *J Phys Chem B* **107**:5768–5772
- Miller MM, Lazarides AA (2005) Sensitivity of metal nanoparticle surface plasmon resonance to the dielectric environment. *J Phys Chem B* **109**:21556–21565
- De Leebeek A et al (2007) On-chip surface-based detection with nanohole arrays. *Anal Chem* **79**:4094–4100
- Tu MH, Sun T, Grattan KTV (2012) Optimization of gold-nanoparticle-based optical fibre surface plasmon resonance (SPR)-based sensors. *Sensor Actuat B-Chem* **164**:43–53

14. Zhang X et al (2012) Sensors based on plasmonic-photonic coupling in metallic photonic crystals. *Sensors* 12:12082–12097
15. Okamoto T, Yamaguchi I, Kobayashi T (2000) Local plasmon sensor with gold colloid monolayers deposited upon glass substrates. *Opt Lett* 25:372–374
16. Lee S, Mayer KM, Hafner JH (2009) Improved localized surface plasmon resonance immunoassay with gold bipyramid substrates. *Anal Chem* 81:4450–4455
17. Chen C-D, Cheng S-F, Chau L-K, Wang CRC (2007) Sensing capability of the localized surface plasmon resonance of gold nanorods. *Biosens Bioelectron* 22:926–932
18. Wang H, Brandl DW, Le F, Nordlander P, Halas NJ (2006) Nanorice: a hybrid plasmonic nanostructure. *Nano Lett* 6:827–832
19. Lee J, Hasan W, Odom TW (2009) Tuning the thickness and orientation of single Au pyramids for improved refractive index sensitivities. *J Phys Chem C* 113:2205–2207
20. Grigorenko AN et al (2006) Antisymmetric plasmon resonance in coupled gold nanoparticles as a sensitive tool for detection of local index of refraction. *Appl Phys Lett* 88:124103–124105
21. Mayer KM, Hafner JH (2011) Localized surface plasmon resonance sensors. *Chem Rev* 111:3828–3857
22. The Dow Chemical Company (2010) Refractive Index of Glycerine-Water Solutions at 20 °C (69 °F)
23. Iqbal T, Afsheen S (2015) Plasmonic band gap: role of the slit width in 1D metallic grating on higher refractive index substrate. *Plasmonics*. doi:10.1007/s11468-015-0122-0
24. Palik ED (1985) Handbook of optical constants of solids. Academic Press, New York
25. Homola J (2003) Present and future of surface plasmon resonance biosensors. *Anal Bioanal Chem* 377:528–539
26. Zhang X et al (2006) Metallic photonic crystals based on solution-processible gold nanoparticles. *Nano Lett* 6:651–655
27. Pearce K, Wang F, Reece PJ (2011) Dark-field optical tweezers for nanometrology of metallic nanoparticles. *Opt Express* 19:25559–25569
28. Pacifici D, Lezec HJ, Atwater HA, Weiner J (2008) Quantitative determination of optical transmission through subwavelength slit arrays in Ag films: Role of surface wave interference and local coupling between adjacent slits. *Phys Rev B* 77:115411–115415
29. Lochbihler H (1994) Surface polaritons on gold-wire gratings. *Phys Rev B* 50:4795–4801
30. Xie Y, Zakharian AR, Moloney JV, Mansuripur M (2005) Transmission of light through a periodic array of slits in a thick metallic film. *Opt Express* 13:4485–4491
31. Porto JA, Garcia-Vidal FJ, Pendry JB (1999) Transmission resonances on metallic gratings with very narrow slits. *Phys Rev Lett* 83:2845–2848
32. Cao Q, Lalanne P (2002) Negative role of surface plasmons in the transmission of metallic gratings with very narrow slits. *Phys Rev Lett* 88:057403
33. De Ceglia D, Vincenti MA, Scalora M, Akozbek N, Bloemer MJ (2011) Plasmonic band edge effects on the transmission properties of metal gratings. *AIP Advances* 1:032151–032165
34. Pang L, Tetz KA, Fainman Y (2007) Observation of the splitting of degenerate surface plasmon polariton modes in a two-dimensional metallic nanohole array. *Appl Phys Lett* 90:111103–111105
35. Pang L, Hwang GM, Slutsky B, Fainman Y (2007) Spectral sensitivity of two-dimensional nanohole array surface plasmon polariton resonance sensor. *Appl Phys Lett* 91:123112–123114
36. Mock JJ, Smith DR, Schultz S (2003) Local refractive index dependence of plasmon resonance spectra from individual nanoparticles. *Nano Lett* 3:485–491
37. Javaid M, Iqbal T (2015) Plasmonic band gap in 1D metallic nano structured devices. *Plasmonics*. doi:10.1007/s11468-015-0025-0 (2015).
38. Iqbal T (2015) Propagation length of surface plasmon polaritons excited by a 1D plasmonic grating. *Curr Appl Phys* 15:1445–1452